JACS
JOURNAL OF THE AMERICAN CHEMICAL SOCIETY
Article
Cite This: J. Am. Chem. Soc. 2018, 140, 285−290
pubs.acs.org/JACS

A Machine-Driven Hunt for Global Reaction Coordinates of Azobenzene Photoisomerization

Pedram Tavadze,*[,†] Guillermo Avendaño Franco,[†] Pengju Ren,[‡,§] Xiaodong Wen,[‡,§] Yongwang Li,[‡,§] and James P. Lewis*[,†]

[†]Department of Physics and Astronomy, West Virginia University, Morgantown, West Virginia 26506-6315, United States
[‡]State Key Laboratory of Coal Conversion, Institute of Coal Chemistry, Chinese Academy of Sciences, Taiyuan, Shanxi 030001, China
[§]Synfuels China Co. Ltd., Huairou, Beijing 101407, China

Supporting Information

ABSTRACT: Azobenzene is a very important system that is often studied for better understanding light-activated mechanical transformations via photoisomerization. The central C−N═N−C dihedral angle is widely recognized as the primary reaction coordinate for changing *cis*- to *trans*-azobenzene and vice versa. We report on a *global reaction coordinate* (containing all internal coordinates) to thoroughly describe the reaction mechanism for azobenzene photoisomerization. Our global reaction coordinate includes *all* of the internal coordinates of azobenzene contributing to the photoisomerization reaction coordinate. We quantify the contribution of each internal coordinate of azobenzene to the overall reaction mechanism. Finally, we provide a detailed mapping on how each significantly contributing internal coordinate changes throughout the energy profile (from *trans* to transition state and subsequently to *cis*). In our results, the central C−N═N−C dihedral remains the primary internal coordinate responsible for the reaction coordinate; however, we also conclude that the disputed inversion-assisted rotation is *half* as important to the overall reaction mechanism and the inversion-assisted rotation is driven by four adjacent dihedral angles C−C−N═N with very little change to the adjacent C−C−N angles.

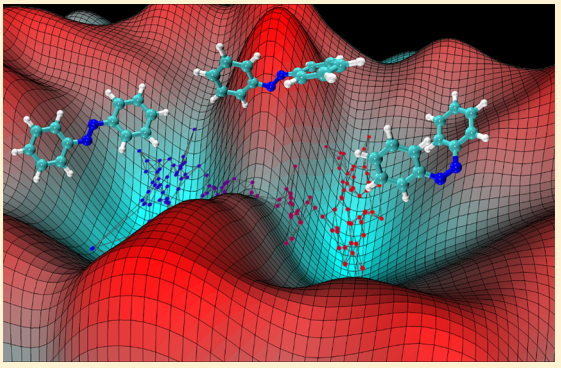

Structurally, azobenzene molecules exist in closed and open forms, which can be interconverted between their *cis*- and *trans*-isomers via light irradiation (photoisomerization). Each isomer has distinct spectral and geometric properties that allow these molecules to serve as ideal model systems for molecular transducers in light-driven devices and optical switches.[1−8] A detailed description of the photoisomerization process, especially in azobenzene, remains elusive, despite a plethora of novel applications and considerable theoretical and experimental studies. There are four proposed mechanisms for isomerization in azobenzene based on experimental and theoretical observations: rotation, inversion, concerted inversion, and inversion-assisted rotation.[9−13] In the rotational pathway (shown in Figure 1), the N═N π-bond breaks, allowing for free rotation around the N−N bond,[9] and the C−N═N−C dihedral angle changes, while the N═N−C angles remain fixed at ∼120°. In the inversion mechanism (also shown in Figure 1), the C−N═N−C angle remains fixed at 0°, but one of the N═N−C angles increases to 180°.[10] A linear transition state is produced in the concerted inversion mechanism when both N═N−C bond angles increase to 180°. Finally, in the inversion-assisted rotation mechanism, there are large changes in both the C−N═N−C angle and the N═N−C angles, simultaneously. No barrier exists along the rotational pathway after excitation into the S1 state. According to previous computational research, the conical intersection between the $S_0$and S_1 states exists when the C−N═N−C dihedral angle is ∼90° and the N═N−C angle is ∼140°. These facts have prompted the acceptance of rotation as the dominant mechanism with concerted inversion occurring under rotation-restricted conditions. Recent simulations have also predicted isomerization of azobenzene through a pedal-like motion of the nitrogen atoms.[14−16]

The greatest challenge in determining reaction coordinates from chemical processes is to sort out the complexity of the reaction pathway. Experimental spectroscopic techniques may pinpoint one or two internal coordinates that will contribute to a specific reaction pathway; however, it is difficult to probe the contributions of all internal coordinates to the reaction coordinate. Herein, we report on a *comprehensive* reaction coordinate describing the photoisomerization reaction mechanism of azobenzene. Azobenzene consists of 116 internal coordinates (bonds, angles, and dihedral angles), and through a series of machine-driven algorithms, we can rank order all of

Received: September 19, 2017
Published: December 13, 2017

DOI: 10.1021/jacs.7b10030
J. Am. Chem. Soc. 2018, 140, 285−290

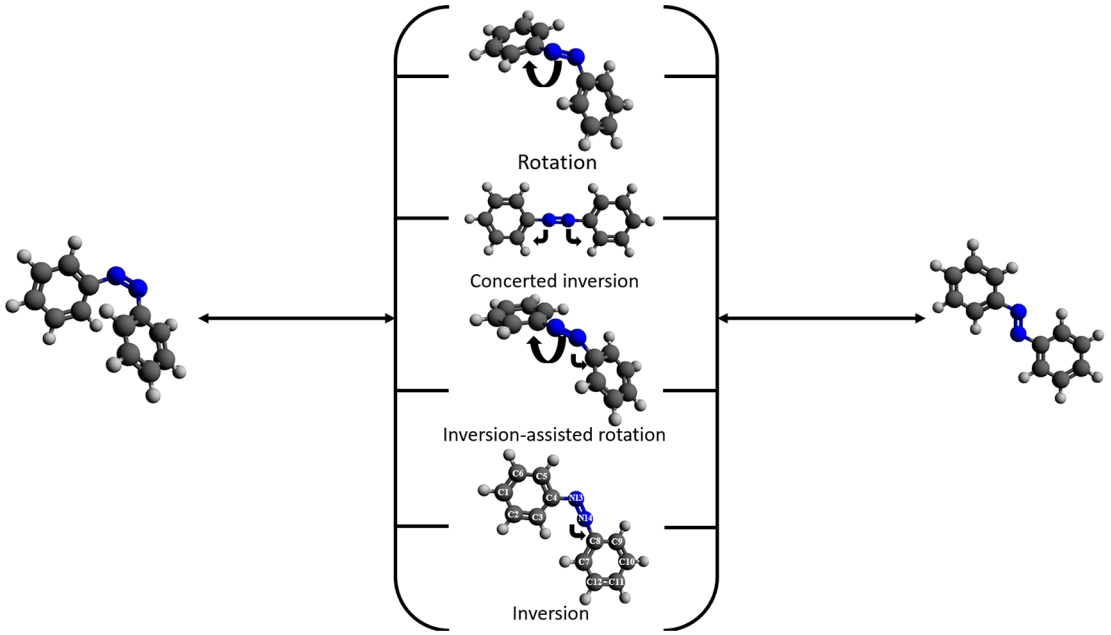

Figure 1. Four reported mechanisms in azobenzene photoisomerization.

these internal coordinates and quantify their contribution to the reaction mechanism of azobenzene photoisomerization. Thereby, in this work, we present a reaction mechanism profile that is based on *all degrees of freedom* of azobenzene.

Many different transition-state-searching algorithms have been proposed since Fukui's early work on the topic, where he introduced the concept of intrinsic reaction coordinates.[17] Some algorithms only require initial points and utilize gradients (the dimer method, the Lanczos iterative method, the Rayleigh−Ritz minimization),[18−21] while other approaches utilize kinetic transition path sampling methods in an attempt to throw "ropes over mountain passes, in the dark".[22−24] Generally, many proposed methods have extreme difficulty searching for barriers in complex systems and are sensitive to local minima. Transition-state-searching algorithms generally yield the geometry of the transition state, or saddle-point of the potential energy surface, but determining global reaction coordinates from intermediates to the transition state is still computationally elusive. The nudged elastic band approach has enjoyed recent popularity in determining reaction pathways, and this method, while very robust and parallelizable, requires a "chain of states" that must be guessed by the user. Generally, machine-driven probabilistic approaches to evaluate the reaction coordinates are more promising in that the reaction pathways need not be chosen *a priori*.[25]

Harnessing the photoisomerization process and increasing its applicability to a variety of materials and systems requires a deeper theoretical understanding of the underlying reaction mechanisms. Density functional theory and molecular dynamics provides direct access to electronic and dynamic processes on the atomic scale and will semiquantitatively ascertain the properties of materials. To accurately simulate the photoisomerization processes, one must go beyond ground-state (Born−Oppenheimer) calculations and include non-adiabatic coupling between the electronic and vibrational states. We have successfully implemented nonadiabatic couplings and a surface-hopping algorithm within a real-space density functional theory approach that utilizes local orbitals (more details are shared in the Supporting Information).[26] We have already demonstrated the effectiveness of our approach by performing molecular dynamics simulations of the cis−trans photoisomerization in azobenzene upon excitation to the S_1 state. By generating an ensemble of trajectories, we gathered characteristic transformation times and quantum yields that we previously compared with ultrafast spectroscopic experiments.[27,28] Additionally, the efficiency of our local orbital density-functional theory code[29] allows us to collect ensemble data large enough to identify the phonon modes that drive relaxation and isomerization.

Machine-driven algorithms are only feasible when very large data sets are available; small data sets increase statistical anomalies. Fortunately, what we have recognized through our previously reported investigations is that low quantum yields in photoactivated events necessitate creating ensembles of 100s of simulations, each starting from a different initial condition. In our previous approaches for understanding photoisomerization through nonadiabatic molecular dynamics (NAMD) simulations, we have used large data sets from ensembles consisting of 100s of simulations (and histograms from these data sets) to implicitly surmise reaction coordinates (e.g., mechanisms in azobenzene photoisomerization). Accordingly, what we have recognized is that these data sets that we have generated (numbering 100 000s of data points) are extremely ideal for applying statistical, probabilistic perspectives. Recently, we have applied machine-driven algorithms on our very large data sets created from nonadiabatic molecular dynamics ensembles to analyze and predict reaction coordinates responsible for inducing photoisomerization in azobenzene.

In our machine-driven hunt for global reaction coordinates, we have developed the following procedure: (1) calculate the mutual information between energy and coordinate data sets generated from nonadiabatic molecular dynamics simulations, as this will quantitatively yield a weight of how each internal coordinate participates in the global reaction coordinate; (2) filter out redundancies of internal coordinate participation in the global reaction coordinate utilizing principal component analysis; (3) build nodes belonging to a network where each node is multidimensionally represented by the highest

DOI: 10.1021/jacs.7b10030
J. Am. Chem. Soc. 2018, 140, 285−290

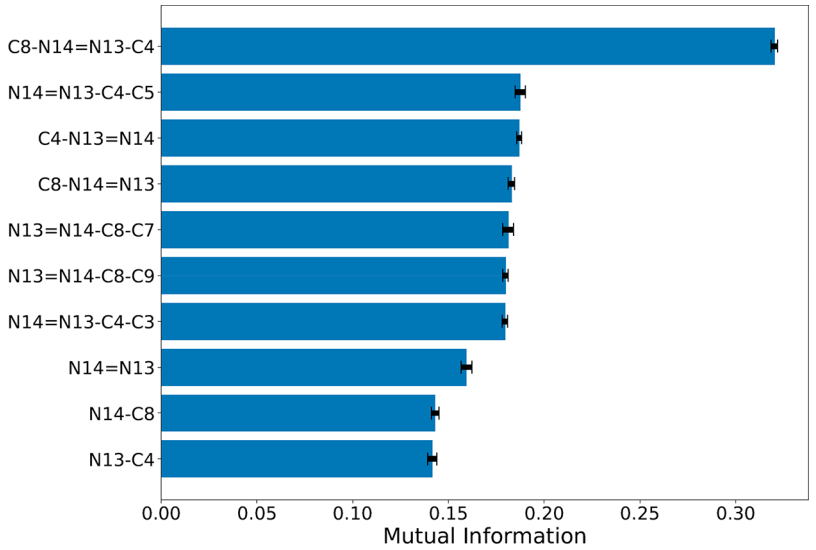

Figure 2. Mutual information for the highest ranking internal coordinates in azobenzene photoisomerization.

occupied molecular orbital (HOMO) energy and that energy's corresponding internal coordinates weighted by the mutual information; and (4) determine global reaction coordinates along the network following the paths of least action. We follow trajectories along these nodes that represent points from molecular dynamics simulations; however, these simulations do not connect one node to another node—the nodes are independent.

Mutual information (MI) is a measure of the (entropic) correlation between two data sets [discussed in the Supporting Information (SI)]. We build data sets from nonadiabatic molecular dynamics simulations to examine the mutual information by first defining the internal coordinates (similar to a Z-matrix[30] representation) as the attributes of our system. A data set includes all the bonds, angles, and dihedrals corresponding to each time step. For example, in our NAMD simulations of azobenzene we build a matrix of 400 000 data sets (rows)—each containing 116 columns of attributes (columns)—from an ensemble of 100 simulations at 300 K (50 simulations starting from the *cis*-conformation and 50 simulations starting from the *trans*-conformation) where each simulation has 4000 time steps and the 116 attributes define the 116 internal coordinates representing all bonds, angles, and dihedrals of the azobenzene molecule. Similarly, we designed another data set, a matrix of 400 000 rows a single column containing HOMO. A necessary condition for a conical intersection is that the two potential energy surfaces should nearly cross, or in other words, the nonadiabatic coupling probability (which determines the probability for a transition) is related to the inverse of the energy differences.[26] For photoisomerization to occur, an electron relaxes from the LUMO to the HOMO; therefore, we are interested in tracking the HOMO and discovering how the internal coordinates correlate to the HOMO.

We rank order the MI data for the largest MI values, shown as a bar chart in Figure 2 (the entropic correlations between all internal coordinates and the HOMO are listed in Table SI1, SI). From our MI rankings, we discover the following: (1) the largest contribution to the change in the HOMO potential energy surface is the C8−N14═N13−C4 dihedral angle (atom labels defined in Figure 1) with MI = 0.32. (2) The next-highest values are the adjacent dihedral angles N13═N14−C8−C7, N13═N14−C8−C9, N14═N13−C4−C5, and N14═N13−C4−C3, all with MI ∼ 0.18. Utilizing principle component analysis (discussed in the Supporting Information), we determine that there are redundancies found in the four dihedral angles: the dihedral angle N13═N14−C8−C9 is redundant to the dihedral angle N13═N14−C8−C7 and the dihedral angle N14═N13−C4−C3 is redundant to the dihedral angle N14═N13−C4−C5. (3) The internal coordinates following with approximately same MI are the angles C4−N13═N14 and C8−N14═N13. (4) the fourth ranking internal coordinates are the N═N double bond and the neighboring N−C bonds, all with MI ∼ 0.15.

These results are remarkable in that by merely considering entropic correlations the primary reaction coordinate for the photoisomerization consists of the C8−N14═N13−C4 dihedral angle; this result is well-known and verified by experiment and theory. However, more than this putative result, our machine-driven results also suggest that there are two other mechanisms involved that rank high in the MI correlations: one mechanism is a concerted motion including the dihedral angle N13═N14−C8−C7 (or its redundant dihedral angle N13═N14−C8−C9) with the angle C8−N14═N13 and the second mechanism is a concerted motion including the dihedral angles N14═N13−C4−C5 (or its redundant dihedral angle N14═N13−C4−C3) together with the angle C4−N13═N14. That is, using mutual information, we are able to predict that the global reaction coordinate mainly includes a rotation around the C8−N14═N13−C4 dihedral angle as well as the rotation-inversion mechanism involving the two angles C4−N13═N14 and C8−N14═N13 and their corresponding dihedral angle. We previously reported, in our ensemble simulations for azo-functional systems,[28] that there is statistically significant assistance from an inversion-assisted rotation (the nonadiabatic coupling vectors of these angles are not negligible) and results of this inversion-assisted rotation mechanism are also reported from experimental observations.[11,31,32] Finally, by calculating the mutual information, we are also able to explicitly evaluate the contribution of each internal coordinate to the reaction coordinate. All 116 internal coordinates of azobenzene contribute something to the reaction coordinate; however, the value of MI for the remaining internal coordinate

DOI: 10.1021/jacs.7b10030
J. Am. Chem. Soc. 2018, 140, 285−290

contributions are greatly reduced compared to the first seven internal coordinates discussed above.

After performing the mutual information calculations, questions remain: Are there redundancies in the data? Can degrees of freedom, or attributes, be removed from the data? Primarily, for the example of azobenzene, do all four dihedral angles (N13═N14−C8−C7, N13═N14−C8−C9, N14═N13−C4−C5, and N14═N13−C4−C3) contribute equally to the photoisomerization reaction coordinate? Do both rotation-inversion mechanisms involving the angles C4−N13═N14 and C8−N14═N13 simultaneously play a role in the reaction coordinate? We filter out redundancies in any of these internal coordinates to the reaction coordinate mechanism by applying principal component analysis (PCA), which will enable us to merge any correlations and further reduce the dimensionality of our attributes (see further details in the Supporting Information). However, before applying PCA, we first reduce the dimensions by choosing only the k attributes that have the highest MI values. Of these k attributes, some of these may be redundant internal coordinates, which will be discovered through PCA. After applying PCA to the azobenzene data set, we then find that the dihedrals N13═N14−C8−C7 and N13═N14−C8−C9 are indeed correlated and N14═N13−C4−C5 and N14═N13−C4−C3 are indeed correlated. In many respects this makes perfect sense; in an inversion-assisted rotation mechanism, the angle C4−N13═N14 (or angle C8−N14═N13) rotates to assist in the change of the primary dihedral C8−N14═N13−C4, which contains the N═N double bond. The rotation of the angle C4−N13═N14 is equally assisting changes in both of the dihedral angles N13═N14−C8−C7 and N13═N14−C8−C9; therefore, it would be repetitive to include both of these internal coordinates in the analysis of the reaction coordinates.

Calculating the mutual information and filtering using principle component analysis only recommends those internal coordinates involved in the reaction mechanisms and their degree of participation (correlation) to the potential energy surface. All 166 internal coordinates contribute to the photoisomerization reaction coordinate of azobenzene, and we can represent the potential energy surface with respect to all 116 degrees of freedom. However, we greatly reduce the dimensionality for representing the potential energy surface by choosing only the top five internal coordinates that contribute the most significantly after calculating mutual information and principle component analysis: the dihedral angle C8−N14═N13−C4, the dihedral angles N13═N14−C8−C7 and N14═N13−C4−C5 (or redundant partners, the dihedral angles N13═N14−C8−C9 and N14═N13−C4−C3), and the two angles C4−N13═N14 and C8−N14═N13. From this reduced dimensionality, we have built a network representing the potential energy surface as a function of this 5-fold dimensionality. As an example, our figure accompanying the abstract shows a reduced potential energy surface for the energy surface projected in the direction of the two primary internal coordinates.

In azobenzene photoisomerization, instead of calculating the distance of a given point with the entirety of the data set of n points, we calculate the distance only with 50 nearest neighbors and then remove the edges that connect nodes with distances less than a predetermined threshold. The distances are calculated using a Euclidian distance that is weighted by the recalculated MI. Once we have built a network with nodes and edges, we can find the nodes corresponding to two optimized structures for local minima and use well-known algorithms to find the shortest path between minima. The Networkx package[33] provides different algorithms to calculate the shortest path, and the best method is Dijkstra's algorithm.[34] After finding the shortest path, we create a list of nodes that need to be passed from the starting node to reach the final node. To avoid outlier data points in the data set (e.g., data points generated from system with high kinetic energy after transition), the initial and final points are chosen from an optimized structure, because it will be unfavorable for Dijkstra's algorithm to choose data points for the path from outliers. Once we have the shortest path, then we have all the features and the energies corresponding to each node; putting these features together will provide the reaction coordinate and the change in the energy via photoisomerization.

We note three regions in the HOMO energy level in Figure 3—two are minima and one is a maximum. The minima of the

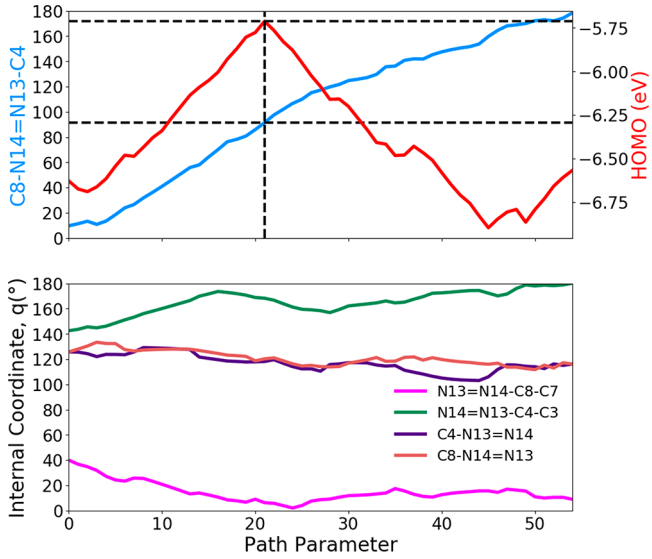

Figure 3. Reaction coordinates (internal coordinates with the largest mutual information and after principle component analysis) are plotted with respect to the HOMO energy's path of least action for azobenzene photoisomerization. (Top) The C8−N14═N13−C4 azobenzene dihedral starts in the cis-isomer and ends in the trans-isomer as the path is followed. (Bottom) Four other major internal coordinates (two dihedrals N13═N14−C8−C7 and N14═N13−C4−C3 and two angles C4−N13═N14 and C8−N14═N13) contribute significantly to the path of least action, offering evidence that an inversion-assisted rotation mechanism to the photoisomerization reaction pathway is mostly influenced by changes in the two dihedral internal coordinates rather than the C−N═N angles.

HOMO correspond to the two forms of azobenzene, *cis* and *trans*. The maximum of the HOMO is the point corresponding to the transition between *cis* and *trans*. The structure at this transition point is a representative structure correspond to the intermediate state as *cis* photoisomerizes to *trans* or vice versa. If we follow the path of least action along the HOMO energy (described in the Supporting Information; we build a surface network and follow the least-action gradients), then we arrive at the pathways shown in Figure 3. Only the five primary, and nonredundant, internal coordinates responsible for the photoisomerization mechanism are plotted. The top plot of Figure 3 also shows how the C8−N14═N13−C4 dihedral changes with respect to the change in the HOMO energy level.

DOI: 10.1021/jacs.7b10030
J. Am. Chem. Soc. 2018, 140, 285−290

Looking at the C8−N14═N13−C4 dihedral, we find that the dihedral tends to 0° for the *cis*-azobenzene, tends to 180° for the *trans*-azobenzene, and is ∼90° for the transition structure; these results are exactly what is putatively supported based on experimental results.

The changing dihedral angle is the primary mechanism anticipated; however, from the plots, we see that other internal coordinates are also contributing to the reaction mechanism. For instance, there are noticeable changes in the two dihedral angles, N13═N14−C8−C7 and N14═N13−C4−C3, and the two angles, C4−N13═N14 and C8−N14═N13 (and, by symmetry, the two dihedral angles N13═N14−C8−C9 and N14═N13−C4−C5), which is supported by the mutual information ranking. However, these dihedral angles and principle angles, near the central dihedral, do not change significantly, as we note in Figure 3. The two dihedrals (N13═N14−C8−C7 and N14═N13−C4−C3) only change by roughly 20° and the two angles (C4−N13═N14 and C8−N14═N13) change only by roughly 10°. According to the mutual information ranking, these internal coordinates indeed contribute to the global reaction coordinate; however, the internal coordinates do not change significantly. This suggests that there certainly is an inversion-assisted rotation mechanism (a concerted motion of the dihedral angles and principal angles); however, this mechanism is not as strongly pronounced as suggested in previous observations. Our results do not support a purely inversion or a concerted inversion mechanism; there is nothing in the reaction coordinate plots of Figure 3 to support these mechanisms.

In conclusion, many researchers have proposed methods for calculating reaction coordinates,[35−41] and some are automated.[42,43] What we propose is unique in that our method evaluates a global reaction coordinate that is *absolutely unbiased*; we merely take *n* data sets that are results from nonadiabatic molecular simulations and perform machine-learning algorithms on this data. The reaction coordinates of the system are automated output. All decisions within our approach, other than fixing the threshold of the mutual information for building the network, are "human-free". Algorithms can easily be put into place to remove this threshold decision as well. Finally, it is very important to note that the reaction coordinates are temperature dependent; we can easily run the simulations at different temperatures to evaluate temperature dependencies.

Our results from mutual information shows the capability of choosing the importance of bonds in a reaction, such as the N═N bond and C−N bonds. The applicability of this method to any other type of transition, such as bond breakage, depends on the output of the simulation package. Our approach is independent of DFT package utilized, as long as the electronic structure calculations can provide an ensemble of simulations with the designated type of transition of interest, the energy eigenvalues mutual information can be calculated, and the network of the potential energy surface can find the shortest path from two different points for any reaction.

■ ASSOCIATED CONTENT

Supporting Information

The Supporting Information is available free of charge on the ACS Publications website at DOI: 10.1021/jacs.7b10030.

A more detailed explanation of the computational methodology (PDF)

■ AUTHOR INFORMATION

Corresponding Authors

*petavazohi@mix.wvu.edu

*james.lewis@mail.wvu.edu

ORCID

Pedram Tavadze: 0000-0001-5238-3689

Xiaodong Wen: 0000-0001-5626-8581

James P. Lewis: 0000-0002-6724-3483

Notes

The authors declare no competing financial interest.

■ ACKNOWLEDGMENTS

J.P.L. acknowledges funding from DOE SC-0004737 and funding from the Chinese Academy of Sciences President's International Fellowship Initiative (PIFI) for 2017. X.W. is grateful for the financial support from the National Natural Science Foundation of China (No. 21473229, 91545121), and Synfuels China, Co. Ltd., also acknowledges National Thousand Young Talents Program of China, Hundred-Talent Program of Chinese Academy of Sciences, and Shanxi Hundred-Talent Program. R.P. is grateful to the funding support from China Postdoctoral Science Foundation (No. 2016M590216). We thank T.E. Steinberger, who provided some insight that greatly assisted the research. We also acknoweldge use of the high-performance computing resources at West Virginia University.

■ REFERENCES

(1) Ikeda, T.; Tsutsumi, O. *Science* **1995**, *268*, 1873−1875.

(2) Berg, R. H.; Hvilsted, S.; Ramanujam, P. S. *Nature* **1996**, *383*, 505−508.

(3) Rau, H. *Photochromism: Molecules and Systems*; Elsevier Science Amsterdam, 2003; p 1218.

(4) Volgraf, M.; Gorostiza, P.; Numano, R.; Kramer, R. H.; Isacoff, E. Y.; Trauner, D. *Nat. Chem. Biol.* **2006**, *2*, 47−52.

(5) Kumar, A. S.; Ye, T.; Takami, T.; Yu, B.-C.; Flatt, A. K.; Tour, J. M.; Weiss, P. S. *Nano Lett.* **2008**, *8*, 1644−1648.

(6) Pathem, B. K.; Zheng, Y. B.; Payton, J. L.; Song, T.-B.; Yu, B.-C.; Tour, J. M.; Yang, Y.; Jensen, L.; Weiss, P. S. *J. Phys. Chem. Lett.* **2012**, *3*, 2388−2394.

(7) Zheng, Y. B.; Payton, J. L.; Chung, C.-H.; Liu, R.; Cheunkar, S.; Pathem, B. K.; Yang, Y.; Jensen, L.; Weiss, P. S. *Nano Lett.* **2011**, *11*, 3447−3452.

(8) Zheng, Y. B.; Payton, J. L.; Song, T.-B.; Pathem, B. K.; Zhao, Y.; Ma, H.; Yang, Y.; Jensen, L.; Jen, A. K. Y.; Weiss, P. S. *Nano Lett.* **2012**, *12*, 5362−5368.

(9) Magee, J. L.; Shand, W.; Eyring, H. *J. Am. Chem. Soc.* **1941**, *63*, 677−688.

(10) Curtin, D. Y.; Grubbs, E. J.; McCarty, C. G. *J. Am. Chem. Soc.* **1966**, *88*, 2775−2786.

(11) Rau, H.; Lueddecke, E. *J. Am. Chem. Soc.* **1982**, *104*, 1616−1620.

(12) Crecca, C. R.; Roitberg, A. E. *J. Phys. Chem. A* **2006**, *110*, 8188−8203.

(13) Bandara, H. M. D.; Burdette, S. C. *Chem. Soc. Rev.* **2012**, *41*, 1809−1825.

(14) Böckmann, M.; Doltsinis, N. L.; Marx, D. *Phys. Rev. E* **2008**, *78*, 036101.

(15) Böckmann, M.; Doltsinis, N. L.; Marx, D. *J. Phys. Chem. A* **2010**, *114*, 745−754.

(16) Bockmann, M.; Marx, D.; Peter, C.; Site, L. D.; Kremer, K.; Doltsinis, N. L. *Phys. Chem. Chem. Phys.* **2011**, *13*, 7604−7621.

(17) Fukui, K. *J. Phys. Chem.* **1970**, *74*, 4161−4163.

(18) Henkelman, G.; Jónsson, H. *J. Chem. Phys.* **1999**, *111*, 7010−7022.

DOI: 10.1021/jacs.7b10030
J. Am. Chem. Soc. 2018, 140, 285−290

(19) Olsen, R. A.; Kroes, G. J.; Henkelman, G.; Arnaldsson, A.; Jónsson, H. *J. Chem. Phys.* **2004**, *121*, 9776−9792.
(20) Zeng, Y.; Xiao, P.; Henkelman, G. *J. Chem. Phys.* **2014**, *140*, 044115.
(21) Xiao, P.; Wu, Q.; Henkelman, G. *J. Chem. Phys.* **2014**, *141*, 164111.
(22) Bolhuis, P. G.; Chandler, D.; Dellago, C.; Geissler, P. L. *Annu. Rev. Phys. Chem.* **2002**, *53*, 291−318.
(23) Rohrdanz, M. A.; Zheng, W.; Clementi, C. *Annu. Rev. Phys. Chem.* **2013**, *64*, 295−316.
(24) Chill, S. T.; Henkelman, G. *J. Chem. Phys.* **2014**, *140*, 214110.
(25) Pozun, Z. D.; Hansen, K.; Sheppard, D.; Rupp, M.; Müller, K.-R.; Henkelman, G. *J. Chem. Phys.* **2012**, *136*, 174101.
(26) Abad, E.; Lewis, J. P.; Zobac, V.; Hapala, P.; Jelinek, P.; Ortega, J. *J. Chem. Phys.* **2013**, *138*, 154106−8.
(27) Neukirch, A. J.; Shamberger, L. C.; Abad, E.; Haycock, B. J.; Wang, H.; Ortega, J.; Prezhdo, O. V.; Lewis, J. P. *J. Chem. Theory Comput.* **2014**, *10*, 14−23.
(28) Neukirch, A. J.; Park, J.; Zobac, V.; Wang, H.; Jelinek, P.; Prezhdo, O. V.; Zhou, H.-C.; Lewis, J. P. *J. Phys.: Condens. Matter* **2015**, *27*, 134208.
(29) Lewis, J. P.; Jelínek, P.; Ortega, J.; Demkov, A. A.; Trabada, D. G.; Haycock, B. J.; Wang, H.; Adams, G.; Tomfohr, J. K.; Abad, E.; Wang, H.; Drabold, D. A. *Phys. Status Solidi B* **2011**, *248*, 1989−2007.
(30) Gordon, M. S. a.; Pople, J. A. *J. Chem. Phys.* **1968**, *49*, 4643−4650.
(31) Rau, H. *J. Photochem.* **1984**, *26*, 221−225.
(32) Cattaneo, P.; Persico, M. *Phys. Chem. Chem. Phys.* **1999**, *1*, 4739−4743.
(33) Hagberg, A. A.; Schult, D. A.; Swart, P. J. Exploring Network Structure, Dynamics, and Function Using Networkx. In *SciPy 2008*; Varoquaux, G., Vaught, T., Millman, J., Eds.; 2008; pp 11−15.
(34) Viswanath, S.; Kreuzer, S. M.; Cardenas, A. E.; Elber, R. *J. Chem. Phys.* **2013**, *139*, 174105.
(35) Carr, J. M.; Trygubenko, S. A.; Wales, D. J. *J. Chem. Phys.* **2005**, *122*, 234903.
(36) E, W.; Vanden-Eijnden, E. *Annu. Rev. Phys. Chem.* **2010**, *61*, 391−420.
(37) Májek, P.; Elber, R. *J. Chem. Theory Comput.* **2010**, *6*, 1805−1817.
(38) Kirmizialtin, S.; Elber, R. *J. Phys. Chem. A* **2011**, *115*, 6137−6148.
(39) Zhang, X.-J.; Liu, Z.-P. *Phys. Chem. Chem. Phys.* **2015**, *17*, 2757−2769.
(40) van Erp, T. S.; Moqadam, M.; Riccardi, E.; Lervik, A. *J. Chem. Theory Comput.* **2016**, *12*, 5398−5410.
(41) Gagorik, A. G.; Savoie, B.; Jackson, N.; Agrawal, A.; Choudhary, A.; Ratner, M. A.; Schatz, G. C.; Kohlstedt, K. L. *J. Phys. Chem. Lett.* **2017**, *8*, 415−421.
(42) Li, W.; Ma, A. *Mol. Simul.* **2014**, *40*, 784−793.
(43) Ma, A.; Dinner, A. R. *J. Phys. Chem. B* **2005**, *109*, 6769−6779.

DOI: 10.1021/jacs.7b10030
J. Am. Chem. Soc. 2018, 140, 285−290